Measurements and Analysis for the Second-Order Statistical Properties of Time-Variant A2G Channels

Kai Mao[1,2], Taiya Lei[1], Yanheng Qiu[1], Qiuming Zhu[1(✉)], Maozhong Song[1], and Yang Miao[2]

[1] Key Laboratory of Dynamic Cognitive System of Electromagnetic Spectrum Space, College of Electronic and Information Engineering, Nanjing University of Aeronautics and Astronautics, Nanjing 211106, China
{maokai,leitaiya,qiuyanheng,zhuqiuming,smz108}@nuaa.edu.cn

[2] The Radio Systems, Faculty of Electrical Engineering Computer Science and Mathematics (EEMCS), University of Twente, Enschede, The Netherlands
y.miao@utwente.nl

Abstract. Channel measurements are the fundamental to accurately learn the realistic channel properties. In this paper, we demonstrate our latest UAV-aided air-to-ground (A2G) channel sounder. Several channel data processing methods, i.e., system response elimination (SRE), sampling time offset compensation (STOC), and multi-path component recognition (MPCR) are also proposed to increase the accuracy of measured channel properties. Moreover, the second-order statistical properties of channel small-scale fading (SSF) such as autocorrelation function (ACF), cumulative distribution function (CDF), and level crossing rate (LCR) are derived based on the measurement data. Finally, time-variant properties of second-order statistics are analyzed according to the measurement data obtained at 3.5 GHz in a near-urban scenario. The results can be used for validating the performance of channel models and assisting the design of A2G communication systems under the similar scenario.

Keywords: A2G communication · channel measurement · channel model · second-order statistical properties

1 Introduction

Unmanned aerial vehicle (UAV) has been widely used on many applications such as military reconnaissance, earthquake relief, forest fire detection, emergency rescue, etc., due to its flexible deployment, high mobility, and low cost. UAV communication technology becomes an important part in the beyond fifth generation (B5G) and sixth generation (6G) communication networks with the ability to build line-of-sight (LoS) links easily [1,2]. It is vital to establish a good communication link to ensure the effectiveness and reliability of the UAV communication system by well understanding the propagation channels. Compared with traditional terrestrial communications, the air-to-ground (A2G) communication

Q. Liang et al. (Eds.): CSPS 2022, LNEE 874, pp. 280–287, 2023.
https://doi.org/10.1007/978-981-99-2362-5_35

has more obvious time-variant channel properties [3]. Channel measurement is the most accurate way to capture the realistic channel. Therefore, it is crucial to carry out A2G channel measurements and analyze the channel properties.

The vector network analyzer (VNA) is a common instrument used to measure the frequency domain characteristics of wireless channel, and the channel impulse response (CIR) can be obtained by using inverse fast Fourier transform (IFFT) [4]. This method has high system reliability but is hard to be utilized to measure A2G channel due to the bulkiness of VNA and the limitation of measurement distance resulting from the wire connection between the link ends and the same VNA. Therefore, separate transceivers are more often used in the A2G channel measurements. Recently, A2G channel measurement campaigns have gained a lot of attentions [5–8]. For example, some portable A2G channel sounders were designed and developed for the platforms as the quadcopter UAV [5], hexacopter UAV [6,7], and octocopter UAV [8]. However, there are still many challenges needed to be tackled. Firstly, the sampling time offset (STO) of transceivers due to the deviation of crystal oscillators could lead to power loss on the sliding correlation results [9]. Secondly, a constant noise threshold is often used to extract the valid multi-path components (MPCs) from the continuous CIR, which is likely to remove low-power multi-paths or bring in some fake multi-paths [10,11]. The last but not least, only few research works analyzed the second-order statics of A2G channel small-scale fading (SSF) in detail [12,13], where there are still some gaps.

To address these issues and fill the gaps, an A2G measurement system with several channel data pre-processing methods, i.e., system response elimination (SRE), STO compensation (STOC), and MPC recognition (MPCR) is proposed and verified in this paper. Moreover, several second-order statistics of channel SSF are derived based on the discrete measurement data, and time-variant second-order statistics are analyzed in a near-urban measurement scenario. In Sect. 2, the developed channel measurement system and target measurement scenario are given. In Sect. 3, we propose several channel data processing methods and derive the second-order statistics of channel SSF. The time-variant properties of second-order statistics based on the measurement data are analyzed in Sect. 4. Section 5 draws the conclusions.

2 Measurements Setup

2.1 Measurement System

The developed channel measurement system consists of two parts, i.e., transmitter (TX) part and receiver (RX) part, as shown in Fig. 1. In the TX part, several components are mounted at the bottom of a hexa-copter UAV including a customized TX software-defined-radio (SDR) module with light weight and small volume, a high-power amplifier, an omnidirectional TX antenna, and a L1-band globe positioning system (GPS) module with GPS antenna. The Zadoff-Chu (ZC) sequence with good autocorrelation property is generated in the TX SDR module as the sounding signal. In the RX part, it consists of an adjustable antenna array, a group of low-noise amplifiers and NI SDR modules, a L1-band

GPS module with GPS antenna, and a high-rate disk array. The antenna array includes four omnidirectional antennas in the azimuth plane and four in the elevation plane, respectively. The high-rate disk array is used to store the raw channel data for subsequent data processing. Both the SDR modules in transceiver support maximum frequency band 6 GHz and maximum bandwidth 100 MHz. It should be mentioned that the GPS modules are not only used to record the locations of transceiver but also used to generate the triggering signal for time synchronization of transceiver.

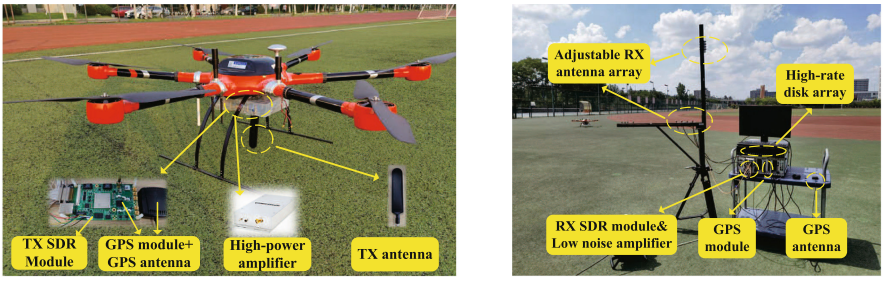

(a) (b)

Fig. 1. (a) TX part and (b) RX part of A2G measurement system.

2.2 Measurement Scenario

As shown in Fig. 2, the measurement campaigns are carried out at 3.5 GHz in a near-urban scenario at the Jiangjun Road campus, Nanjing University of Aeronautics and Astronautics, Nanjing, China. In this measurement scenario, the average height of the buildings and trees are about 20 m and 5 m, respectively. The RX is put on the toproof of a building with height of 25 m, which is a typical height of base station. The UAV flies forward along a straight line with the velocity of 2 m/s at the height of 60 m, from the starting point to the end point as shown in Fig. 2. During the measurement, the line-of-sight (LoS) path always exists. The non-LoS (NLoS) propagation paths could also occur caused by the ground reflection or the scattering of surrounding buildings and trees.

3 Data Processing and Channel Statistical Properties

3.1 Channel Data Pre-processing

After obtaining the raw channel measurement data, the sliding correlation operation can be used to extract time-variant CIRs [7]. However, the original CIRs involves the effect of system response caused by the hardware modules, i.e., filters, amplifiers, and so on. Therefore, we obtain the system response by performing a back-to-back measurement before the real measurement, where the system response is denoted as $G(t)$ in frequency domain. Assuming the transmitted sounding signal and the received signal are denoted as $s(t)$ and $y(t)$,

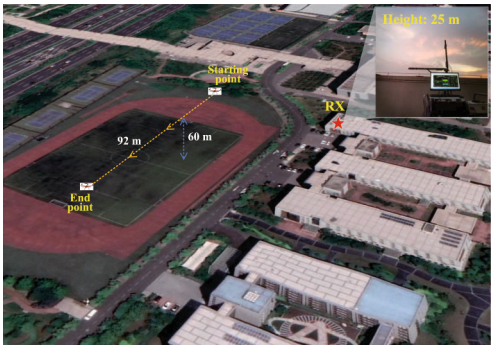

Fig. 2. Measurement scenario.

respectively, the CIR after SRE can be expressed as

$$h_{SRE}(t) = \text{IFFT}\left(\frac{Y(t) \cdot \hat{S}^*(t)}{G(t)}\right) \tag{1}$$

where IFFT $(\cdot)$ is the inverse Fourier transform, $Y(t)$ is the Fourier transform of $y(t)$. and $\hat{S}^*(t)$ is the Fourier transform of $\hat{s}^*(t)$, where $\hat{s}^*(t)$ is the conjugate reverse sequence of $s(t)$.

Moreover, we find that there are STOs between the transceiver due to the deviation of crystal oscillator, which would bring maximum cumulative error of 6 dB to the sliding correlation peaks (SCPs). In [9], a signal recovery method is proposed to compensate the error of SCPs caused by the STO. However, the dynamic range of measured CIR decreases a lot by using this method, where the measured CIR could lose some resolvable channel multipath. Therefore, we propose a modified STOC method as

$$h_{STOC}(t) = \int_{t-W_r}^{t+W_r} h_{SRE}(t) \cdot \text{sinc}\left(\frac{k}{I}\right) dk \tag{2}$$

where W_r is the window size, and I is the oversampling ratio of sinc filter.

After obtaining the CIR, another important thing is recognize the valid MPCs from the complete CIR. The constant noise threshold is normally used to recognize the MPCs but it could bring some fake paths or remove some valid paths. In this paper, the constant false alarm rate method with dynamic threshold is applied for MPCR, where the dynamic threshold can be expressed as

$$Thr(t) = \frac{\xi}{W_d - W_g}\left(\int_{t-\frac{W_d}{2}}^{t-\frac{W_g}{2}} h_{STOC}(w)\, dw + \int_{t+\frac{W_g}{2}}^{t+\frac{W_d}{2}} h_{STOC}(w)\, dw\right) \tag{3}$$

where W_d and W_g are the width of detection window and guard window, respectively, and $\xi = (W_d - W_g) \cdot \left(p^{-1/(W_d - W_g)} - 1\right)$ is the threshold factor, where p is the probability of false alarm. Then the parameters of CIR peaks larger than the threshold are taken as the values of valid paths such as path amplitude $\alpha_n(t)$.

3.2 Second-Order Statistical Properties of Channel SSF

Second-order statistical properties of channel fading are common parameters for describing the statistical properties of fading channels and validating the performance of channel models [14,15], which are also important for the channel coding, channel estimation, interleave scheme in the communication system. Considering the channel measurement data in the channel sounder is discrete, we derive several second-order statistics of channel SSF in a discrete way in this section, i.e., ACF, CDF, and LCR. The channel fading can be seen as the superposition of large-scale fading (LSF) and SSF. Therefore, the discrete SSF can be expressed by removing the LSF from the envelope of received signal as

$$\gamma[m] = \frac{|y[m]|}{\sum_{n=1}^{N[\lceil m/l_s \rceil]} \sqrt{|\alpha_n[\lceil m/l_s \rceil]|^2}} \tag{4}$$

where m is the diecrete time index, $y[m]$ is the discrete received signal, $\lceil \cdot \rceil$ is the floor function, and l_s is the length of sounding sequence. $N[\lceil m/l_s \rceil]$ is the valid path number in $\lceil m/l_s \rceil$ th CIR, $\alpha_n[\lceil m/l_s \rceil]$ is the path amplitude of nth path in $\lceil m/l_s \rceil$ th CIR. ACF is an important second-order statistical property to reflect the similarity change of channel SSF along with time delay Δt. The ACF of channel SSF can be expressed as

$$R_{\gamma\gamma}[\Delta t; m] = \sum_{k \in [m, m+l_s]} \gamma[k]\gamma[k - \Delta t]. \tag{5}$$

It should be mentioned that the length of SSF signal in (5) should be infinite according to the original definition of ACF. However, due to the length limitation of real measurement data and the non-stationarity of A2G channel, the length of SSF signal is set as the length of sounding signal to perform the autocorrelation operation in this paper. The CDF with respect to specific threshold level r can be expressed as

$$\begin{aligned} F_\gamma[r; m] &= \Pr(\gamma[k] \le r)_{k \in [m, m+K]} \\ &= \frac{\text{card}\{k | \gamma[k] \le r, k \in [m, m+K]\}}{K} \end{aligned} \tag{6}$$

where K is the sampling number of one statistical interval, card $\{\cdot\}$ is the element number of a vector. LCR represents the times that channel SSF positively or negatively passes through a specific level in unit time. The LCR with respect to specific threshold level r can be expressed as

$$L_\gamma[r; m] = \frac{\text{card}\{k | \gamma[k] \le r, \gamma[k] > r, k \in [m, m+K]\}}{KT_s} \tag{7}$$

where T_s is the sampling rate.

4 Measurement Results Analysis

For the measurement scenario in Sect. 2.2 we continuously record 20480 samples of raw received signals to calculate one slice of channel SSF. In total 460 slices

are recorded with time interval of 100 ms. The sampling rate of received signals is 100 Msps. Then the time-variant second-order statistics of channel SSF, i.e., ACF, CDF, and LCR are calculated and analyzed in this section.

As shown in Fig. 3(b), we present three ACFs for three slices of channel SSF at different time instants, i.e., t= 0 s, 20 s, and 40 s. Each ACF for different slice of channel SSF has different decreasing tendency, which means the ACFs are time variant. However, the ACF only decreases to about 0.8 in each slice duration. Therefore, we further calculate the ACF between the first slice and all the other slices of channel SSF along the whole measurement trajectory. It can be found that the lowest ACF is about 0.6, which means that the channel SSF always keeps high correlation in this measurement case.

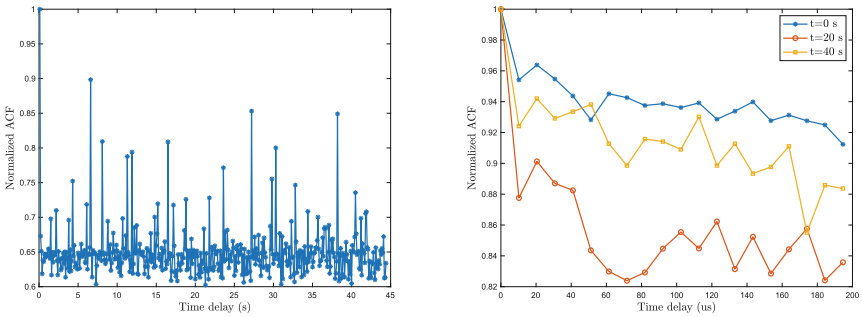

(a) (b)

Fig. 3. (a) ACF along the whole measurement trajectory and (b) time-variant measured ACFs within three different slices.

Similarly, it can be found from Fig. 4(a) that the CDFs are also time-variant. To clearly show the results, we only plot 20 slices with time interval of 0.3 s. As the CDF reflects the distribution of fading amplitude, 99.74% of maximum CDF value (denoted as 99.74% CDF) is an important parameter for calculating the fading depth. The fading amplitudes corresponding to each 99.74% CDF are shown in Fig. 4(b), which are time-variant as well and mainly distribute between 0–4.7 dB in this measurement scenario.

LCR is another second-order statistic relative to fading amplitude, which reflects the times that fading envelope positively or negatively pass through a specific threshold level in unit time. As shown in Fig. 5(b), the LCRs are also time-variant, but most of the threshold levels corresponding to the maximum values of LCR for each slice of channel SSF distribute between 0–3 dB, which does not vary too much from the 0 dB of the whole measurement trajectory. And the crossing times of different slice of LCR distribute between $3 \cdot 10^6$–$4.8 \cdot 10^6$, which is also close to $4 \cdot 10^6$ for the whole measurement. Therefore, the LCRs do not vary too much along the whole measurement, which means this measurement scenario is not highly non-stationary.

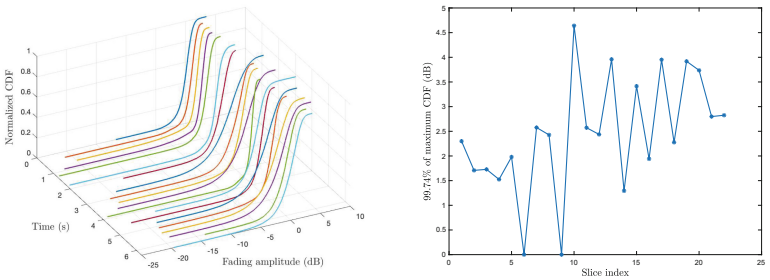

(a) (b)

Fig. 4. (a) Time-variant measured CDFs and (b) fading amplitude corresponding to 99.74% CDF.

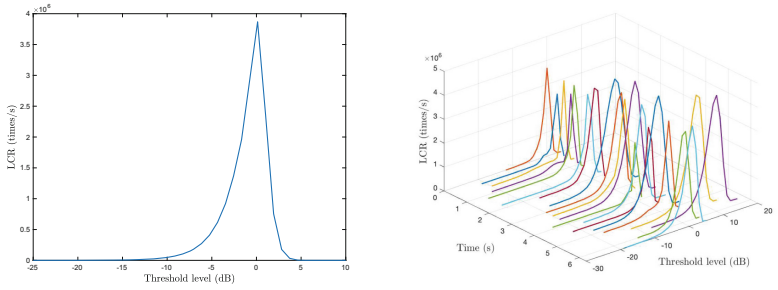

(a) (b)

Fig. 5. (a) LCR for the whole measurement trajectory and (b) time-variant measured LCRs for different slices.

5 Conclusion

This paper has developed a UAV-aided channel sounder, where several optimized channel data processing methods, i.e., SRE, STOC, and MPCR have been proposed. Moreover, several second-order statistics of channel SSF have been derived and analyzed based on the measurement data. The results have shown that the second-order statistics of A2G channel are time-variant. The channel SSF can keep above 60% similarity in the whole measurement, the fading amplitudes corresponding to each 99.74% CDF distribute between 0–4.7 dB, and most of the threshold level corresponding to the maximum value of each LCR distribute between 0–3 dB. These results would be a good reference to the channel coding, channel estimation, interleave scheme of A2G communication system. In the future, we plan to develop more efficient real-time channel data processing methods to increase the sampling interval of CIRs.

Acknowledgments. This work was supported in part by the National Natural Science Foundation of China (No. 62271250), in part by China Scholarship Council, and

in part by Postgraduate Research & Practice Innovation Program of Jiangsu Province, No. KYCX22_0360.

References

1. You, X., Wang, C.-X., Huang, J., Gao, X., Zhang, Z., et al.: Towards 6G wireless communication networks: Vision, enabling technologies, and new paradigm shifts. Sci. China Inf. Sci. **64**(1), 1–74 (2021)
2. Zhu, Q., Bai, F., Pang, M., Li, J., Zhong, W., Chen, X., et al.: Geometry-based stochastic line-of-sight probability model for A2G channels under urban scenarios. IEEE Trans. Antennas Propag. **70**(7), 5784–5794 (2022)
3. Mao, K., Zhu, Q., Song, M., Li, H., Ning, B., et al.: Machine learning-based 3D channel modeling for U2V mmWave communications. IEEE Int. Things J. **9**(18), 17592–17607 (2022)
4. Lyu, Y., Kyösti, P., Fan, W.: Sub-THz VNA-based channel sounder structure and channel measurements at 100 and 300 GHz. In: Proceedings of PIMRC 2021, Helsinki, Finlan, pp. 1–5 (Sept 2021)
5. Khawaja, W., Ozdemir, O., Erden, F., Guvenc, I., Matolak, D.W.: Ultra-wideband air-to-ground propagation channel characterization in an open area. IEEE Trans. Aerosp. Electron. Syst. **56**(6), 4533–4555 (2020)
6. Rodríguez-Piñeiro, J., Domínguez-Bolaño, T., Cai, X., et al.: Air-to-ground channel characterization for low-height UAVs in realistic network deployments. IEEE Trans. Antennas Propag. **69**(2), 992–1006 (2021)
7. Ning, B., Li, T., Mao, K., et al.: A UAV-aided channel sounder for air-to-ground channel measurements. Physical Commun. **47**, 101366 (2021)
8. Geise, R., Weiss, A., Neubauer, B.: Modulating features of field measurements with a UAV at millimeter wave frequencies. In: Proceedings of CAMA 2018 Västerås, Sweden, pp. 1–4 (Sept 2018)
9. Burmeister, F., Jacob, R., Traßl, A., Schwarzenberg, N., Fettweis, G.: Dealing with fractional sampling time offsets for unsynchronized mobile channel measurements. IEEE Wirel. Commun. Lett. **10**(12), 2781–2785 (2021)
10. Meng, Y.S., Lee, Y.H.: Measurements and characterizations of air-to-ground channel over sea surface at C-band with low airborne altitudes. IEEE Trans. Veh. Technol. **60**(4), 1943–1948 (2011)
11. Cui, Z., Briso-Rodríguez, C., Guan, K., Güvenç, I., Zhong, Z.: Wideband air-to-ground channel characterization for multiple propagation environments. IEEE Antennas Wireless Propag. Lett. **19**(9), 1634–1638 (2020)
12. Simunek, M., Fontan, F.P., Pechac, P., Otero, F.J.D.: Space diversity gain in urban area low elevation links for surveillance applications. IEEE Trans. Antennas Propag. **61**(12), 6255–6260 (2013)
13. Cui, Z., Briso-Rodríguez, C., Guan, K., Zhong, Z., Quitin, F.: Multi-frequency air-to-ground channel measurements and Analysis for UAV communication systems. IEEE Access. **8**, 110565–110574 (2020)
14. Zhu, Q., et al.: Map-based channel modeling and generation for U2V mmwave communication. IEEE Trans. Veh. Technol. **71**(8), 8004–8015 (2022)
15. Chang, H., Wang, C.X., Liu, Y., et al.: A novel nonstationary 6G UAV-to-ground wireless channel model with 3-D arbitrary trajectory changes. IEEE Internet Things J. **8**(12), 9865–9877 (2021)